J Mater Sci (2008) 43:3327–3332
DOI 10.1007/s10853-008-2506-4

Characterization and corrosion protection properties of cerium conversion coating on $Gr_{(f)}$/Al composite surface

Chunyu Wang · Gaohui Wu · Qiang Zhang · Longtao Jiang

Received: 9 September 2007 / Accepted: 29 January 2008 / Published online: 5 March 2008

Abstract The aim of this work is to investigate corrosion protection properties of Ce conversion coating on the graphite fiber-reinforced aluminum matrix ($Gr_{(f)}$/Al) composite surface by electrochemical measurements, and microstructure of the Ce conversion coating was studied by scanning electron microscopy (SEM), energy dispersive X-ray (EDX), and X-ray photoelectron spectroscopy (XPS). It is found that the coating covers the whole surface of $Gr_{(f)}$/Al composites as oxidized islands, since there are some micro-cracks on the coating. The Ce conversion coating consists of Ce-rich nano-particles, and the contact sites between particles have some porosity. The porosity is not obvious during initial deposition, however, as deposition time prolonged development apparently. Moreover, some severe cracks may appear during the drying process, since evaporation of water molecules would cause shrinkage and large stress is induced. In addition, pretreatment of surface has an effect on the formation of cracks. Ce conversion coating has the composition of Ce^{3+} and Ce^{4+}. Deposition of Ce-rich coating on $Gr_{(f)}$/Al composite surfaces shifts the polarization curves toward lower current density values. Electrochemical impedance spectroscopy (EIS) data show that Ce conversion coating improved corrosion resistance as compared with samples that have no coating.

Introduction

Surface treatments are commonly used in metal protection systems in the metal industry. The protection methods used for metal matrix composites are of the same type as those designed for aluminum alloys. Chromate conversion coatings are popular methods of surface treatment for Al or Al matrix composites; however, we know that chromium in hexavalent state is both highly toxic and carcinogenic, and this has led to a search for alternative nontoxic surface treatment methods [1, 2]. Rare earth elements have been regarded as a good alternative for hexavalent chromium, especially in the case of cerium which have two higher oxidation states and are reasonably abundant [3, 4]. In the case of Al and Al matrix composites, the corrosion protection mechanism afforded by cerium incorporated in the surface oxide is believed to involve a decrease in the rate of cathodic oxygen reduction by the precipitation of trivalent cerium hydroxide ($Ce(OH)_3$) at regions of high pH, to form a complex hydrated cerium oxide layer on the cathodic sites [5]. This has been shown clearly for copper-containing aluminum alloys where cerium-rich insoluble films have been identified at copper precipitates; these films precipitate from solutions because of the local increase in alkalinity at the copper cathodic sites [6, 7]. The Ce conversion coating inhibits both the cathodic and anodic reactions rate. From literature [8], the effect of several parameters, such as temperature, time of immersion, cerium ions and hydrogen peroxide concentration, pH of the conversion solution, on the composition and morphology of the conversion coating is investigated, and agglomerates with a "dry-mud" morphology of mixed cerium–aluminum oxide are deposited above the cathodic intermetallic particles, while using a cerium (III) nitrate solution the coating is more uniform but thinner than that obtained with cerium (III) chloride. The pretreatment consisted of desmutting, degreasing, and acid activation had also an effect on the cracks of Ce conversion coatings [9].

C. Wang (✉) · G. Wu · Q. Zhang · L. Jiang
School of Materials Science and Engineering, Harbin Institute of Technology, P.O. Box 433, No. 92 West DaZhi Street, Harbin 150001, P.R. China
e-mail: wcyadam@126.com

High-modulus graphite fiber-reinforced aluminum alloys ($Gr_{(f)}$/Al) composites are regarded as ideal structure materials for excellent mechanical properties; however, the corrosion capacity is much poorer than Al alloys, because the $Gr_{(f)}$/Al composite easily leads to the establishment of a graphite fiber-Al galvanic couple [10–12]. Surface coating can inhibit formation of galvanic couples by isolating electrochemical corrosion medium; so it is important to search protection coatings for $Gr_{(f)}$/Al composites.

The aim of this work is to investigate corrosion protection properties of Ce conversion coating on the $Gr_{(f)}$/Al composite surface by electrochemical measurements, and microstructure characterization of the Ce conversion coating was investigated using scanning electron microscopy (SEM), energy dispersive X-ray (EDX), and X-ray photoelectron spectroscopy (XPS). For comparison, the corrosion behaviors of uncoated $Gr_{(f)}$/Al composite were also studied.

Experimental

The M40 graphite fibers were used as reinforcement and 6061 Al was employed as matrix, which has the composition of (wt%): 0.30Cu, 1.00Mg, 0.70Fe, 0.60Si, 0.15Mn, 0.20Cr, 0.25Zn, 0.15Ti, remainder Al. The $Gr_{(f)}$/Al composite samples were fabricated by the patented squeeze-casting technique, including infiltration of the graphite fiber performed by molten 6061 Al under a pressure of $\sim$100 MPa.

In the present work, the Ce conversion coating process involved the following steps: Polishing with 1000# abrasive paper → wiping with acetone → degreasing in alkaline solution → rinsing with distilled water → polishing with 1:1HNO_3 → rinsing with distilled water → chemical immersion treatment in Ce salt baths → rinsing with distilled water → drying in air. The chemical immersion process of the Ce conversion coating treatment on the $Gr_{(f)}$/Al composite surface was obtained and shown in Table 1.

All the surfaces of specimens were degreased with acetone and then rinsed in distilled water before being used for each electrochemical experiment. The corrosion behavior of the treated samples was evaluated under immersion in 3.5 wt% sodium chloride using the potentiodynamic polarization and electrochemical impedance spectroscopy (EIS). All the experiments were conducted at room temperature (25 °C).

Electrochemical measurements were performed in a three-electrode cell. Area of exposure of the sample diameter was 10 mm. An Ag/AgCl electrode was employed as the reference electrode. The potential of this electrode with respect to standard hydrogen electrode is +0.197 V. Graphite bar was used as counter electrode. All electrochemical experiments were performed after stabilization of free corrosion potential (FCP). In conducting polarization experiments, the potential was scanned from the cathodic to anodic direction at a rate of 0.166 mV/s. Potentiodynamic polarization curves were obtained from −1200 mV to −200 mV from FCP. EIS measurements were performed by applying a sinusoidal potential perturbation of 10 mV at FCP. The impedance spectra were measured with a frequency sweep from 100 kHz to 10 mHz in logarithmic increment. The impedance data were fitted to appropriate equivalent electrical circuit using a complex nonlinear least-squares fitting routine, using both the real and imaginary components of the data.

The resulting coating surface was also characterized using XPS and scanning electro microscope (SEM), and the energy dispersive spectroscopy (EDS) unit attached to the SEM.

Results and discussion

Microstructure

Figure 1 shows a SEM image of the $Gr_{(f)}$/Al composite surface. From Fig. 1, it is can be seen that the graphite fibers combined firmly with Al alloys. Figure 2 shows a SEM image of Ce conversion coating on the $Gr_{(f)}$/Al composite surface. According to EDS analysis, the light-colored nodules has higher content of Ce. The EDS maps of the corresponding element plane are shown in Fig. 3; the Ce content of the coating reached 47.48 wt%. It was found that the coating covered the whole surface of $Gr_{(f)}$/Al composites as oxidized islands, and some micro-cracks were also found on the coating. The micro-cracks were not continuous network; this island-like coating was piled up by spherical cerium-rich particles. The crack initiation is dependent on a number of factors, for example pretreatment of desmutting, degreasing, and acid activation, and

Table 1 The Ce conversion coating treatment on $Gr_{(f)}$/Al composite surface

	Rare earth solution (g/L)	Accelerator (g/L)	Stabilizer (g/L)	pH	Temperature (°C)	Time (min)
Contents of baths	$Ce(NO)_3$	H_2O_2	H_3BO_3	–	–	–
Conditions	3.0–4.0	0.3–0.4	0.03–0.04	3.5–4.5	30 ± 2	120

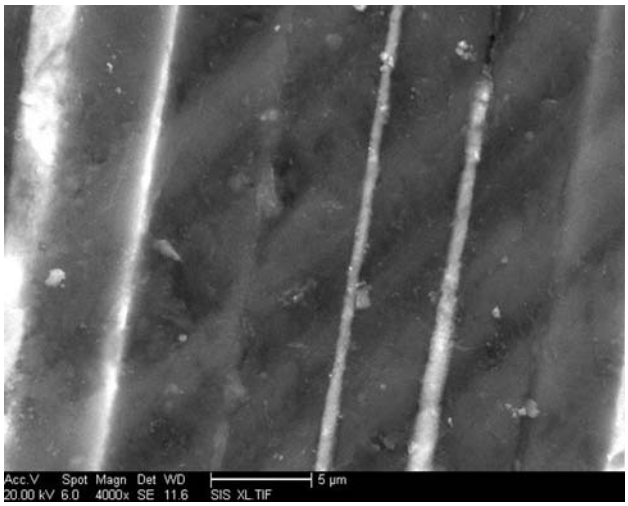

Fig. 1 Surface morphology of the $Gr_{(f)}$/Al composites

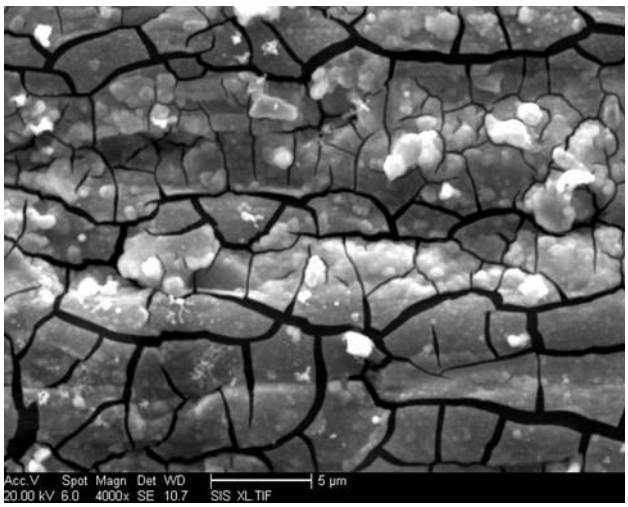

Fig. 2 Surface morphology of the Ce conversion coating on $Gr_{(f)}$/Al composites

other parameters such as temperature, time of immersion, cerium ions and hydrogen peroxide concentration, pH of the conversion solution, and so on, which would affect the composition and morphology [12]. Lin et al. [13] had proposed that cracks in the Ce conversion coating occurred as a result of drying process, and the evaporation of water molecules caused shrinkage in volume, allowing cracks to form. Obviously, the stress as a result of shrinkage increased, and thicker the coating is, larger the stress induced, leading to more severe cracking. From the above statements, the crack of Ce conversion coating is caused by evaporation of water molecules and more severe cracking appears when the coating is thicker. In addition, pretreatment of the surface is effected on formation of cracks.

As reported in previous investigations [14, 15], the rare earth element was deposited over cathodic areas, probably as Ce (Ce^{3+} and Ce^{4+}) hydroxide/oxide, because the precipitation process was driven by the electrochemical potential differences, while Al oxide covered the metal matrix. The cathodic areas on the composite surface had different deposition rates, so they had different coating thickness, leading to the final microstructure.

Deposition characteristic

Microstructure of Ce conversion coating with different immersion times in Ce baths was investigated to find out the formation of micro-cracks, as shown in Fig. 4. It shows that some spherical cerium-rich particles are found on the $Gr_{(f)}$/Al composites when the depositing time is 1 min; local distribution of spherical cerium-rich particles is found when depositing time is 5 min. Micro-crack initiation appeared after 10 min of depositing, and some micro-cracks appear when depositing time is 30 min.

The Ce-rich spherical nano-particles are the main characteristics of Ce conversion coating. Contact sites between particles have some porosity and the porosity is seldom during initial deposition; however, micro-cracks develop apparently with longer depositing time. Moreover, micro-cracks probably originated from inhomogeneous deposition on the different surface sites or the increasing inter-stress of coating during the rapid drying step.

The high-resolution XPS spectra of Ce3d analysis found that Ce^{3+} and Ce^{4+} are present in Fig. 5. Pardo et al. [16] have shown several binding energies of Ce, the characteristic satellite of Ce^{4+} and Ce^{3+}. Other researchers have confirmed the presence of Ce^{4+} compounds in the Ce conversion coatings probably related to atmosphere exposition [17]. The presence of Ce^{3+} ions in the solution promotes the formation of a conversion coating of $Ce(OH)_3$ on several metal surface forming a thick film composed of $Ce(OH)_3$ and Ce_2O_3:

$$Ce^{3+} + 3OH^- \rightarrow Ce(OH)_3,$$

$$2Ce(OH)_3 \rightarrow Ce_2O_3.$$

The presence of H_2O_2, resulting from oxygen reduction, promotes the formation of Ce^{4+} due to oxidation of Ce^{3+} [18]:

$$2Ce^{3+} + H_2O_2 \rightarrow 2Ce^{4+} + 2OH^-.$$

Thus, the Ce conversion coating is composed of Ce^{3+} and Ce^{4+} states as confirmed by XPS results of the Ce-coating sample. The results suggest that oxidation of Ce^{3+} compounds may take place.

$$Ce^{3+} + H_2O \rightarrow Ce(OH)_2^{2+} + 2H^+ + e^-.$$

The Ce conversion coating cannot hinder the hydrogen evolution that takes place during the passivation process due to the formation of Ce coatings on the composite

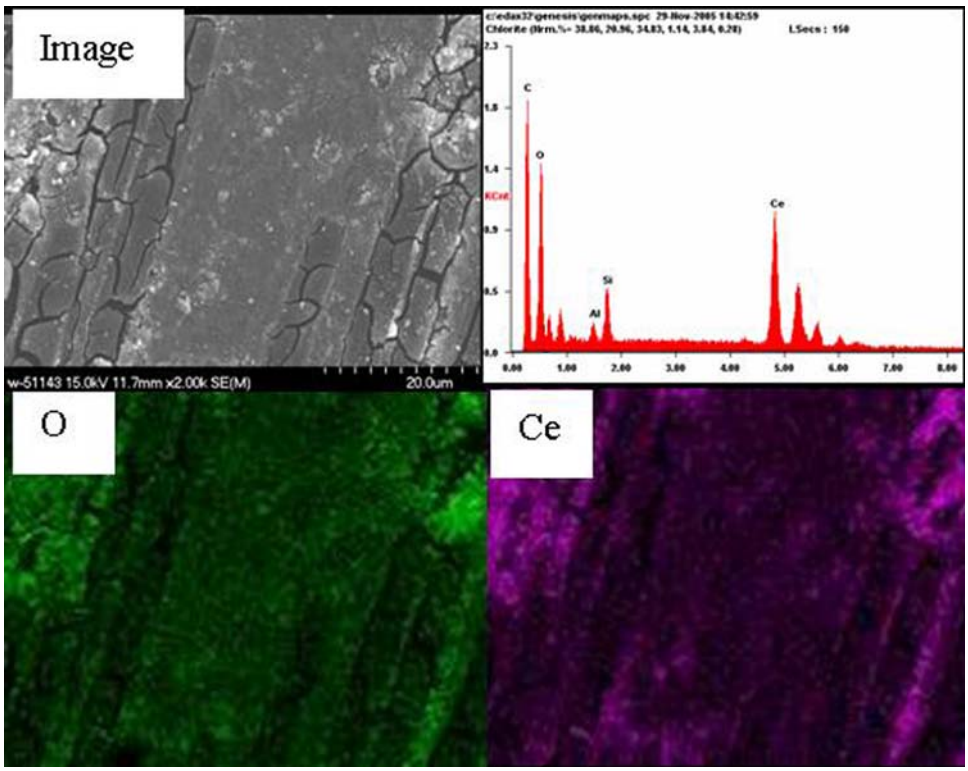

Fig. 3 The element corresponding for Ce conversion coating on $Gr_{(f)}$/Al composite surface

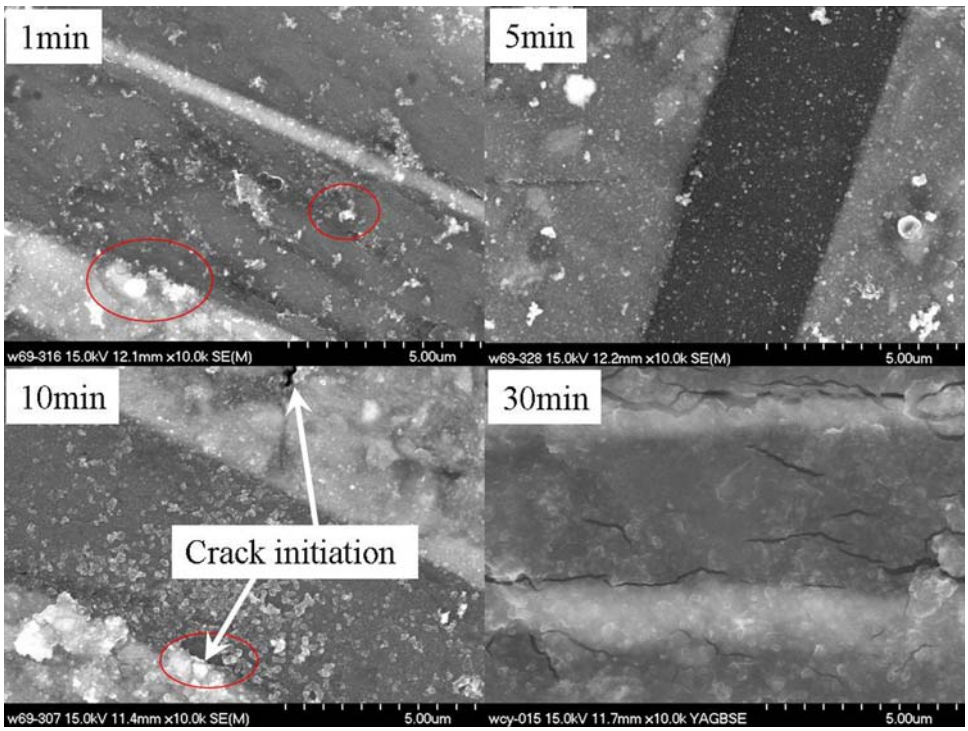

Fig. 4 Different deposition time for procedures of micro-crack formation

surface. The mechanisms involved in corrosion process seem to be slightly different for Ce conversion coatings. The surface of the graphite fiber has a lot of local defects, where the energy is high, leading the Ce deposition chemical reaction to occur easily in there. In general, Ce coatings can be obtained on both Al substrate and graphite fiber surface on $Gr_{(f)}$/Al composites.

From above, it is concluded as follows: the slight solubility of Ce^{3+} and OH^- allows the formation of $Ce(OH)_3$, changed Ce^{3+} ions to $Ce(OH)_2^{2+}$ ions or reverse transition in

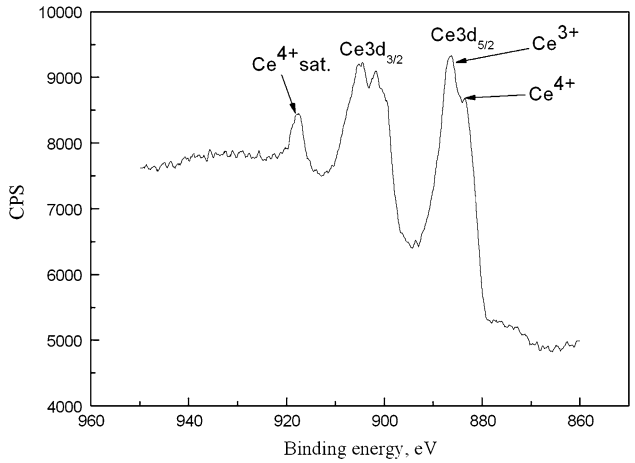

Fig. 5 The high-resolution XPS spectra of Ce3d for Ce conversion coating

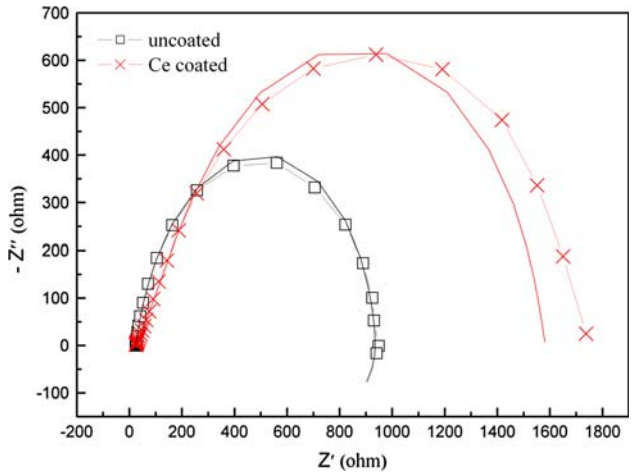

Fig. 6 Nyquist diagrams for coated or uncoated samples

solution which can diffuse reaching local defects. When there is contact with the bare oxidizable metal, these ions reduce to Ce^{3+} and precipitate as $Ce(OH)_3$ (probably together with $Al(OH)_3$). This suggests that the Ce-rich coating was composed of Ce^{3+} and Ce^{4+}.

Corrosion properties

The corrosion properties of coated and uncoated composites in 3.5 wt% NaCl solution was evaluated by EIS and potentiodynamic polarization curves. Figure 6 shows the Nyquist diagrams contrast for coated and uncoated samples. From Fig. 6, it can be seen that the shape of the Nyquist diagrams is similar for both samples, and the shape is like a semicircle. The impedance data are mainly capacitive. The semicircle for the coated sample Nyquist diagram has a larger circle diameter. This indicates that higher corrosion resistance for the coated sample though a relatively lower corrosion resistance was observed for the uncoated sample. The simulation fitting procedure was performed using the equivalent circuit of Fig. 7 and the parameters used are shown in Table 2: where R_s is the solution resistance, C_p is a constant-phase element representing the intact layer, R_p is its polarization resistance [19]. The polarization resistance R_p for the coated sample (2513 Ω), which is much higher than the uncoated sample (1189 Ω), indicates that Ce conversion coating can improve corrosion resistance of $Gr_{(f)}$/Al composites.

For the potentiodynamic polarization curves for the coated and uncoated Gr/Al composites, the experiment is done by immersing in 3.5 wt% NaCl solution at room temperature as shown in Fig. 8. Ce-rich coating on composite surfaces decreased the corrosion current density (i_{corr}), partially blocking the cathodic reaction and shifting

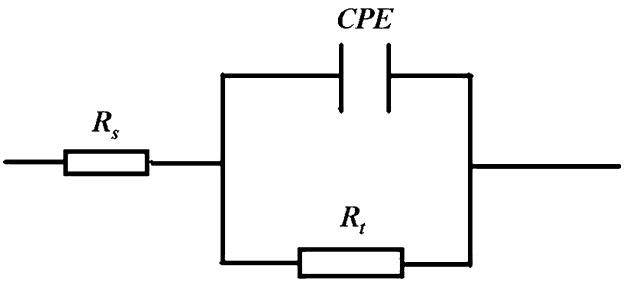

Fig. 7 The equivalent circuit used to model

Table 2 The parameters of equivalent circuits for different treated samples

	R_s (Ω)	R_p (Ω)	C_p (F cm^{-2})
Uncoated sample	32.15	1189	1.87E-5
Coated sample	34.11	2513	5.23E-5

the polarization curves toward lower current density values. Table 3 shows that the uncoated sample has lower E_{corr} (−794 mV) and higher i_{corr} (6.713 μA cm^{-2}); in contrast, the coated sample has higher E_{corr} (−697 mV) and lower i_{corr} (4.923 μA cm^{-2}).

From this work, we know that the cathodic reaction was hindered by the presence of the cerium conversion coatings. When the Ce-coated samples are immersed in the corrosion media, the presence of the cerium conversion coating delays the onset of corrosion activity. The results show that the cerium conversion coating formed on the sample surface delayed the corrosion behavior of $Gr_{(f)}$/Al composites when the composite sample was immersed in corrosion medium. It indicates that Ce conversion coating can improve corrosion resistance clearly for $Gr_{(f)}$/Al composites.

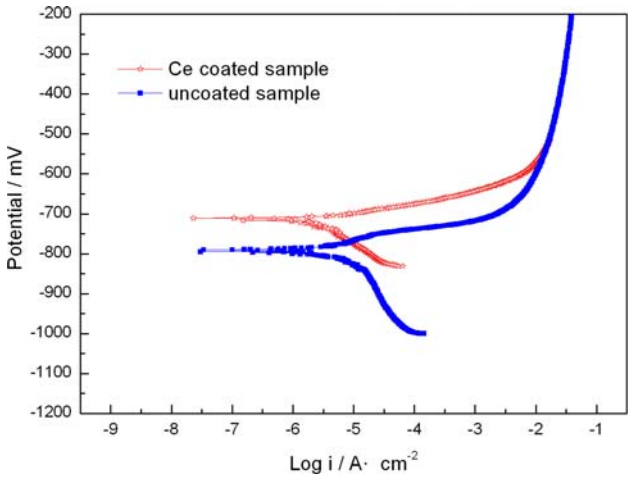

Fig. 8 Potentiodynamic polarization curves of coated or uncoated samples

Table 3 The values of E_{corr} and i_{corr} from potentiodynamic polarization curves

	Uncoated sample	Coated sample
E_{corr}(mV)	−794	−697
Log i_{corr}(A/cm^2)	−5.53	−6.13

Conclusion

From the above research, the coating covered the whole surface of $Gr_{(f)}$/Al composites as oxidized islands, and some micro-cracks were also found on the coating. The EDS maps show that the amount of Ce reached 47.48 wt% in the coating. The Ce-rich spherical nano-particles are the main characteristics of Ce conversion coating. Contact sites between particles have some porosity and the porosity is seldom during initial deposition, however, micro-cracks develop apparently with longer depositing time. Moreover, some severe cracks may appear during the drying process, since evaporation of water molecules would cause shrinkage and large stress is induced. In addition, pretreatment of the surface has effect on the formation of cracks. EIS data show that the Ce conversion coating improved corrosion resistance of the $Gr_{(f)}$/Al composites. Potentiodynamic polarization curves show that the uncoated sample has lower E_{corr} and higher i_{corr}; in contrast, the coated sample has higher E_{corr} and lower i_{corr}. So, we can conclude that Ce conversion coating can improve corrosion resistance distinctly for $Gr_{(f)}$/Al composites.

References

1. Kendig MW, Davenport AJ, Isaacs HS (1993) The mechanism of corrosion inhibition by chromate conversion coatings from X-ray absorption near edge spectroscopy (XANES). Corros Sci 34:41
2. Traverso P, Spiniello R, Monaco L (2002) Corrosion inhibition of Al 6061 T6/Al_2O_3p 10% (v/v) composite in 3.5% NaCl solution with addition of cerium (III) chloride. J Surf Interf Anal 34(1):185
3. Hughes AE, Taylor RJ, Hinton BRW, Wilson L (1995) XPS and SEM characterization of hydrated cerium oxide conversion coatings. J Surf Interf Anal 23(7–8):540
4. Xingwen Y, Chunnan C, Zhiming Y, Derui Z, Zhongda Y (2001) Study of double layer rare earth metal conversion coating on aluminum alloy LY12. J Corros Sci 43:1283
5. Kumar Mishra A, Balasubramaniam R (2007) Corrosion inhibition of aluminum alloy AA 2014 by rare earth chlorides. J Corros Sci 49:1027
6. Davó B, de Damborenea JJ (2004) Use of rare earth salts as electrochemical corrosion inhibitors for an Al–Li–Cu (8090) alloy in 3.56% NaCl. J Electrochim Acta 49:4957
7. Pardo A, Merino MC, Arrabal R, Merino S, Viejo F, Carboneras M (2006) Effect of Ce surface treatments on corrosion resistance of A3xx.x/SiCp composites in salt fog. J Surf Coat Technol 200:2938
8. Dabalà M, Ramous E, Magrini M (2004) Corrosion resistance of cerium-based chemical conversion coatings on AA5083 aluminium alloy. J Mater Corros 55(5):381
9. Fahrenholtz WG, O'Keefe MJ, Zhou H, Grant JT (2002) Characterization of cerium-based conversion coatings for corrosion protection of aluminum alloys. J Surf Coat Technol 155:208
10. Mansfeld F, Jeanjaquet SL 1986 The evaluation of corrosion protection measures for metal matrix composites. J Corros Sci 26(9):727
11. Greene HJ, Mansfeld F (1997) Corrosion protection of aluminum-matrix composites. Corros 53(12):920
12. Wendt RG, Moshier WC, Shaw B et al (1994) Corrosion-resistant aluminum matrix for graphite-aluminum composites. J Corros Sci 50(11):819
13. Lin CS, Fang SK (2005) Formation of cerium conversion coatings on AZ31 magnesium alloys. J Electrochem Soc 152(2):B54
14. Decroly A, Petitjean J-P (2005) Study of the deposition of cerium oxide by conversion on to aluminum alloys. J Surf Coat Technol 194:1
15. Campestrini P, Terryn H, Hovestad A, de Wit JHW (2004) Formation of a cerium-based conversion coating on AA2024: relationship with the microstructure. J Surf Coat Technol 176(3):365
16. Pardo A, Merino MC, Arrabal R, Viejo F (2006) Carboneras M Improvement of corrosion behavior of A3xx.x/SiCp composites in 3.5 wt% NaCl solution by Ce surface coatings. J Electrochem Soc 153(2):B52
17. Aramaki K (2003) XPS and EPMA studies on self-healing mechanism of a protective film composed of hydrated cerium(III) oxide and sodium phosphate on zinc. J Corros Sci 45(1):199
18. Aramaki K (2001) The inhibition effects of cation inhibitors on corrosion of zinc in aerated 0.5 M NaCl. J Corros Sci 43(8):1573
19. Yu XW, Yan CW, Cao CN (2002) Study on the rare earth sealing procedure of the porous film of anodized Al6061/SiC_p. J Mater Chem Phy 76:228